

# Insights Into the High Catalytic Activity of Li-ion Battery Waste Toward Oxygen Reduction to Hydrogen Peroxide

Magdalena Warczak,<sup>\*,[a, b]</sup> Magdalena Osial,<sup>[c]</sup> Weronika Urbańska,<sup>[d]</sup> Natalia Sławkowska,<sup>[a]</sup> Agnieszka Dąbrowska,<sup>[e, f]</sup> Magdalena Bonarowska,<sup>[b]</sup> Marcin Pisarek,<sup>[b]</sup> Roman Minikayev,<sup>[g]</sup> Michael Giersig,<sup>[c]</sup> and Marcin Opallo<sup>[b]</sup>

Developing highly efficient and cost-effective electrocatalysts for oxygen reduction reaction (ORR) in aqueous media is crucial for energy conversion systems such as fuel cells or Zn-air batteries. Electrode materials from spent devices such as lithium-ion batteries (LIBs) are a serious environmental problem. One of the solutions is their reuse for other electrochemical processes. This work demonstrates the application of solid residues of carbon-based powders left over from the hydro-metallurgical recycling process of LIBs' waste as efficient catalysts for ORR. Microscopic and spectroscopic studies of the residue disclosed their porous structure and various cobalt

contents, depending on the recycling procedure. These battery wastes display ORR catalytic activity when deposited at the liquid-liquid and solid electrode-electrolyte interfaces. Scanning Electrochemical Microscopy (SECM) tests showed that assembling battery waste at the liquid-liquid interface boosts the efficiency of H<sub>2</sub>O<sub>2</sub> production by one to two orders of magnitude. The catalytic activity towards 2-electron ORR strongly depends on waste powder compositions and structures, e.g., porosity, heteroatom presence, level of defects, and graphitization.

## Introduction

The slow depletion of fossil fuels and the continuous increase of environmental pollution by combustion products compelled researchers to develop green, renewable energy sources such as fuel cells or metal-air batteries.<sup>[1]</sup> Therefore, the incoming global energy crisis drives research on oxygen electrode reactions such as oxygen reduction reaction (ORR) and oxygen evolution reaction (OER).<sup>[2]</sup> ORR is an essential reaction both in life processes and in energy conversion and storage devices.<sup>[2]</sup> ORR mechanism in an aqueous solution is quite complex, as was first pointed out by Damjanovic et al.<sup>[3]</sup> and later elaborated by Wroblowa.<sup>[4]</sup> In general, ORR follows two pathways: 2-electron reduction to H<sub>2</sub>O<sub>2</sub> and/or 4-electron reduction to H<sub>2</sub>O.<sup>[5]</sup> The product of 2-electron ORR is regarded as a "green" oxidant applied e.g., in chemistry, cosmetics, paper and textile indus-

tries, and was proposed as an alternative fuel for fuel cells,<sup>[6]</sup> whereas a 4-electron ORR is targeted for fuel cells. Therefore, low-cost "green" and mild methods of H<sub>2</sub>O<sub>2</sub> production are highly in demand to replace the harmful to the environment anthraquinone oxidation method.<sup>[7]</sup> Direct H<sub>2</sub>O<sub>2</sub> synthesis from gaseous H<sub>2</sub> and O<sub>2</sub> over the metal catalyst is environmentally acceptable but still not without risk.<sup>[7]</sup> Recently, electrochemical H<sub>2</sub>O<sub>2</sub> synthesis by ORR has been considered a more promising alternative.<sup>[8,9]</sup> Although ORR has been studied for nearly a century, its sluggish kinetics, high overpotential, low faradaic efficiency, and catalyst's stability seem to be the main bottlenecks of this process. This caused a continuous quest for a new ORR catalyst until, recently driven by the development of energy conversion systems.<sup>[10]</sup>

Precious metals such as platinum, palladium, and gold, as well as their alloys with low overpotential, are currently the

[a] Ph. D. M. Warczak, B. Eng. N. Sławkowska  
Faculty of Chemical Technology and Engineering  
Bydgoszcz University of Science and Technology  
Seminarijna 3 Street, 85-326 Bydgoszcz, Poland;  
E-mail: magdalena.warczak@pbs.edu.pl

[b] Ph. D. M. Warczak, Ph. D. M. Bonarowska, Ph. D. Eng. M. Pisarek,  
Prof. M. Opallo  
Institute of Physical Chemistry, Polish Academy of Sciences  
Kasprzaka 44/52 Street, 01-224 Warsaw, Poland

[c] Ph. D. M. Osial, Prof. M. Giersig  
Department of the Theory of Continuous Media and Nanostructures  
Institute of Fundamental Technological Research, Polish Academy of  
Sciences  
Pawińskiego 5B Street, 02-106 Warsaw, Poland

[d] Ph. D. W. Urbańska  
Faculty of Environmental Engineering  
Wrocław University of Science and Technology  
Wybrzeże Wyspiańskiego 27 Street, 50-370 Wrocław, Poland

[e] Ph. D. A. Dąbrowska  
Faculty of Chemistry  
University of Warsaw  
Pasteura 1 Street, 02-093 Warsaw, Poland;

[f] Ph. D. A. Dąbrowska  
Biological and Chemical Research Centre  
University of Warsaw  
Żwirki i Wigury 101 Street, 02-089 Warsaw, Poland

[g] Ph. D. R. Minikayev  
Institute of Physics, Polish Academy of Sciences  
al. Lotników 32/46, 02-668 Warsaw, Poland

Supporting information for this article is available on the WWW under  
<https://doi.org/10.1002/celec.202400248>

© 2024 The Authors. ChemElectroChem published by Wiley-VCH GmbH. This is an open access article under the terms of the Creative Commons Attribution License, which permits use, distribution and reproduction in any medium, provided the original work is properly cited.

most efficient ORR electrocatalysts.<sup>[11]</sup> However, their high price, low abundance, and low durability are serious limitations. On the other hand, transition metals and their oxides are less expensive. When properly engineered, they provide an efficient and stable alternative to noble metals. Cobalt, manganese, copper, and iron oxides are the most prospective candidates.<sup>[12]</sup> Other transition metal compounds, such as metallic compounds, sulfides, selenides, phosphides, nitrides, and molecular and single-atom materials, are employed as ORR catalysts.<sup>[13]</sup> One has to bear in mind that even natural transition metal deposits will be exhausted in the following decades.<sup>[14]</sup> Apart from metallic catalysts, carbon-based materials including carbon nanotubes, graphite felts, and hierarchically porous carbon are utilized as ORR catalysts.<sup>[14,15]</sup> Due to their low cost, abundance, high surface area, good stability, and electrical conductivity, these materials are regarded as promising electrocatalysts for ORR.<sup>[13]</sup> To decrease its overpotential and increase reaction efficiency, carbon materials are doped with heteroatoms (e.g., N, O, B) or non-noble metals.<sup>[13,16–18]</sup> Based on the above, it can be concluded that, due to the cost, occurrence, and catalytic (in many cases synergistic) properties, carbon-based materials modified with transition metals seem to be the most promising ORR electrocatalysts.<sup>[19]</sup> Indeed, transition metal particles together with carbon-based materials are already employed as electrodes in billions of electronic or electric devices, including batteries. Although transition metals are a small fraction of these materials, the problem with their limited natural sources will appear sooner or later.<sup>[20]</sup> Application of the products of battery electrode recycling may be one of the solutions to this problem. Even though this process is mainly oriented towards metal recovery,<sup>[21]</sup> materials left after leaching may retain or acquire electrocatalytic properties, for example, due to the small amount of transition metals left after processing.

Lithium-ion batteries are widely present in our everyday lives. The popularity of portable electronics and electric vehicles generates an increasing amount of toxic waste to be collected and recycled.<sup>[21]</sup> Therefore, there is a high demand for the reuse of the residue carbon-based material left after recovery treatment as a part of global battery waste management. Toxic transition metals and electrolytes from the spent batteries are a threat to health, the environment, and the economy. Therefore, their efficient recovery is highly desirable.<sup>[22]</sup> On the other hand, spent LiBs are a valuable source of various metals, mainly Li, Co, Ni, trace amounts of metals such as Fe, Zn, Cr, Al, Cu, and carbon materials, e.g., graphite.<sup>[23,24]</sup> They can be recovered by hydrometallurgical (acid leaching), and pyrometallurgical methods and direct physical recycling.<sup>[24]</sup> The first method is the most promising and widely developed because it is cheaper and consumes less energy than raw material processing.<sup>[25]</sup> High selectivity and recovery rate, low energy consumption, and high purity of the products are important advantages of this method<sup>[26]</sup> which prompted us to choose it for this work. As leaching agents, both inorganic and organic acids are proposed.<sup>[27–30]</sup> The leaching process is usually assisted by reducing agents that increase the recovery of such metals as Co and Mn.<sup>[31,32]</sup>

The recovered materials from spent LiBs have been recently explored as electrocatalysts for generating compounds considered an alternative source of clean energy.<sup>[33]</sup> The electrocatalytic properties of materials recovered from spent lithium-ion batteries towards ORR were demonstrated.<sup>[33–34]</sup> This seems to be a new trend parallel to the extensive research on biomass waste employment as low-cost alternative catalysts for many electrode reactions, including ORR<sup>[35,36]</sup> that promote sustainable development and circular economy.<sup>[37]</sup>

Recently, we<sup>[34]</sup> and others<sup>[38–40]</sup> demonstrated that the electrode modified with lithium-ion battery waste exhibited electrocatalytic properties towards 2-electron ORR. Contrary to most studies, we utilized in our research the residue carbon-based material obtained directly after the hydrometallurgical recycling process without any additional chemical treatments (e.g., chemical oxidation, additional cobalt, or nitrogen doping).<sup>[41,42]</sup> Furthermore, the same material assembled at a liquid-liquid interface increased the efficiency of biphasic H<sub>2</sub>O<sub>2</sub> generation,<sup>[34]</sup> a proposed alternative to the electrode-electrolyte interface.<sup>[43]</sup> In this work, we focused on the relationship between the structure and chemical composition of battery waste and its (electro)catalytic activity toward ORR to find out the origin of this phenomenon. For this purpose, LiBs' waste was leached in the acidic bath with various combinations of reducing agents (H<sub>2</sub>O<sub>2</sub>, glutaric acid). The solid residue was studied using several spectroscopic and microscopic methods to determine its morphology, porosity, and elemental composition, the structure of carbon components, the presence of metals, and their speciation. Finally, ORR activity of these materials at solid electrode-electrolyte was determined by cyclic voltammetry (CV) and linear scan voltammetry (LSV) at rotating disc electrode (RDE),<sup>[44]</sup> whereas activity at the liquid-liquid interface by scanning electrochemical microscopy (SECM),<sup>[45]</sup> respectively.

## Results and Discussion

**THE MORPHOLOGY AND COMPOSITION ANALYSIS.** Scanning Electron Microscopy (SEM) images (Figure 1) of the residue carbon-based battery waste show well-developed irregular structures with pores of various sizes.

Specific features of the given material depend on the composition of the leaching bath. Granules having a size of 50–100 nm are characteristic of Material 1, obtained in the presence of H<sub>2</sub>O<sub>2</sub> as a reducing agent (Figures 1a, b). These granules agglomerate into larger objects (some as large as 10 μm) with irregular size and shape. Bulk structures with irregular patterns or wrinkles seem to be a graphite-based material,<sup>[40]</sup> while tiny granules may consist of the post-leaching product(s).<sup>[46,47]</sup> Figures 1c–d demonstrate that the replacement of H<sub>2</sub>O<sub>2</sub> in a concentrated H<sub>2</sub>SO<sub>4</sub> bath by glutaric acid changes completely the morphology of the battery waste to large clusters (Material 2). Additionally, tiny granules are less numerous than in Material 1. The addition of both reducing agents to an acidic bath produces well-developed flakes (Material 3) similar to Material 1 (Figures e–f). These flakes have numerous

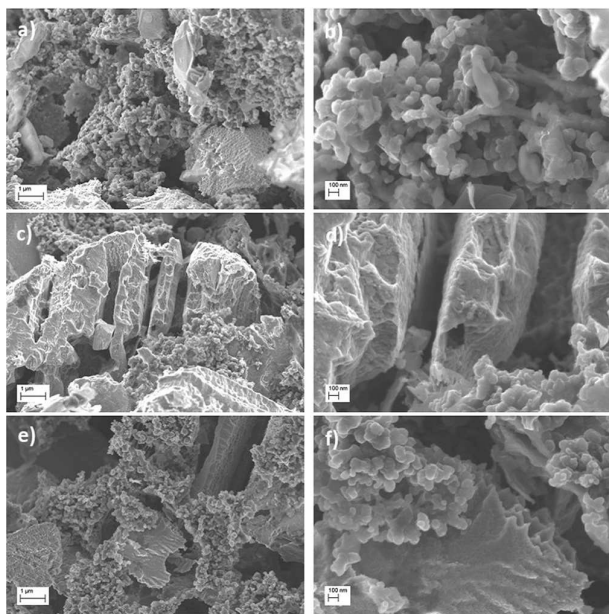


**Figure 1.** SEM images of the post-leaching spent battery powders recorded with different magnifications for (a–b) Material 1, (c–d) Material 2, (e–f) Material 3.

bumps, increasing the surface area. On the other hand, the small granules seen in the images of Materials 1 and 2 are absent.

The elemental maps (Figure 2) indicate the presence of carbon, oxygen, cobalt, and sulfur as the post-leaching residue. The distribution of oxygen correlates with that of cobalt, suggesting the presence of post-leaching cobalt oxides in all materials.

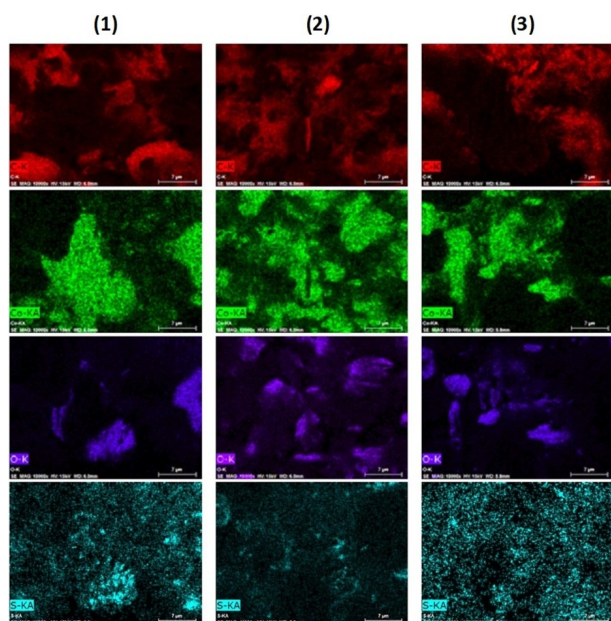


**Figure 2.** Energy Dispersive Spectroscopy (EDS) elemental maps of major constituent elements of Materials (1–3). The colors point to the presence of carbon (red), cobalt (green), oxygen (blue), and sulfur (light blue).

The X-ray Photoelectron Spectroscopy (XPS) survey spectra (Figure 3) indicate the presence of C1s, O1s, P2p, F1s, S2p, Ns1, Co2p and Auger peaks for all Materials, and additionally the Mn2p peak for Material 3.

C1s peaks present in the region from ca. 284 eV to 292 eV are identified as typical for the graphite - the main component of the battery anode.<sup>[48]</sup> After the deconvolution procedure, one can distinguish the highest intensity peak at ca. 284.0 eV corresponding to the carbon atoms forming C–C bonds in the graphite sheets ( $sp^2$ ).<sup>[49]</sup> Another peak in the binding energy range from 285.5 to 286.7 appears, which can be assigned to carbon with  $sp^3$  hybridization, where the carbon atoms are bonded to heteroatoms like oxygen (C–O) or nitrogen (C–N)<sup>[50]</sup> or to hydrogen (C–H).<sup>[51]</sup> Next, peaks in the interval from about 288.0 eV to about 289.7 eV can be ascribed to the carbon of carbonyl C=O and O=C–OH groups (e.g., quinone groups)<sup>[52]</sup> or oxygen functionalities resulting from carbon surface oxidation during leaching.<sup>[50]</sup> In turn, the peak at ca. 291 eV reveals the presence of a C–F bond formed due to the traces of the electrolyte–LiPF<sub>6</sub>.<sup>[53]</sup>

O1s peaks seen at 532.2 eV are characteristic of the C=O bonding, and the following peaks at ca. 534.0, 536.2, and 537.8 eV can be ascribed to the graphite C–O surface groups, suggesting that it was partially modified during the leaching.<sup>[53]</sup> In addition to the characteristic bonds for the carbon and oxygen functional groups, Me–O bonds with an energy of approximately 529.5 eV were also identified. The presence of metal oxides was confirmed by deconvolution of the Co2p and Mn2p spectra (data not shown). The presence of Co<sup>3+</sup> (~780.0 eV) and Co<sup>2+</sup> (~782.0 eV) as well as Mn<sup>4+</sup> (~642.5 eV) and Mn<sup>2+</sup> (~640.8 eV) was detected. Additionally, it was found that the peak at 778.5 eV can be assigned to the cobalt metal state.<sup>[54,55]</sup> As mentioned earlier, the presence of S, P and N was found in the investigated materials, their amount usually do not exceed 0.5 At.%. Despite this, a spectra fitting procedure was performed, and it was concluded that the S 2p peaks seen at

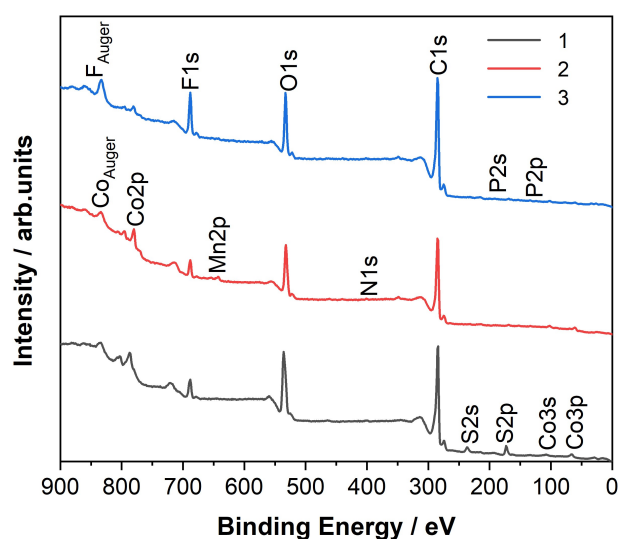


**Figure 3.** XPS survey spectra recorded for Material 1 (grey line), Material 2 (red line) and Material 3 (blue line).

ca. 168.5–169 eV energy are characteristic of sulfate from a leaching bath.<sup>[56]</sup> The F 1s peaks at 688 eV and 689.7 eV indicated the presence of the C–F bonds and LiFP<sub>6</sub>.<sup>[53]</sup> The P2p peaks at c.a. 133.6 eV can be attributed to phosphates or pyrophosphates, which may come from the traces of the electrolyte not being completely washed and decomposed.<sup>[57]</sup> The N1s peaks at c.a. 400 eV can be attributed to the nitrogen forming C–N and C–NH<sub>x</sub> bonds.<sup>[50]</sup> These may come from the N-residue of lithium nitrides formed by the reaction of nitrogen with lithium either at the electrode in a Li-ion battery during charging/discharging processes or during the leaching process under the atmosphere.<sup>[58]</sup>

The elemental composition is similar for all materials based on XPS measurements. The main chemical elements are carbon (76–81.5%) and oxygen 11.6–16.5% (Table S1 in Supporting Information). The content of cobalt varies from 0.7 to 0.2%. Mn (0.2%) is only present in Material 2. Sulfur, nitrogen, phosphorus, fluorine, silicon, and calcium are impurities originating from Li-ion battery electrolyte or leaching medium (Table S1).

The Rietveld method was used to determine the sample fraction content and phase unit cell parameters (see Figure S1 and Table 1). The graphite contents in crystalline phases are 99.1(7) wt.%, 87.9(6) wt.% and 92.0(7) wt.% for Materials 1, 2 and 3, respectively. Lithium cobaltate is the other crystalline component. Importantly, Material 3 contains two different phases – different in stoichiometry. The X-ray Diffraction (XRD) phase analysis indicates that all samples consist of two types of carbon crystalline phases condensed in graphite hexagonal structure (Space Group (S.G.): *P63/mmc*) and lithium cobalt oxide condensed in rhombohedral  $\alpha$ -NaFeO<sub>2</sub> structure (S.G.: *R-3m*) (Table S2).

Although the absolute value of the LiCoO<sub>2</sub> unit cell parameters reported in the literature varies (Table S2), the value of the *c/a* unit cell ratio helps to estimate the stoichiometry of the material. Thus, a *c/a* ratio close to 4.999 is typical for near-stoichiometric materials, and this parameter increases with decreasing Li content.<sup>[59]</sup> In other words, the smaller the amount of Li in the unit cell, the higher the *c/a* observed. Therefore, one may conclude that all lithium cobaltate (LCO) phases in Material 2 and c.a. 43% of LCO in Material 3 are near stoichiometric. On the other hand, the LCO phase in Material 1 and the remaining part of LCO in Material 3 consist of less lithium.

Raman spectra confirmed the presence of both well-structured carbon materials and an amorphous fraction (Figure 4, Table S3). Bands related to amorphous carbon (D bands)

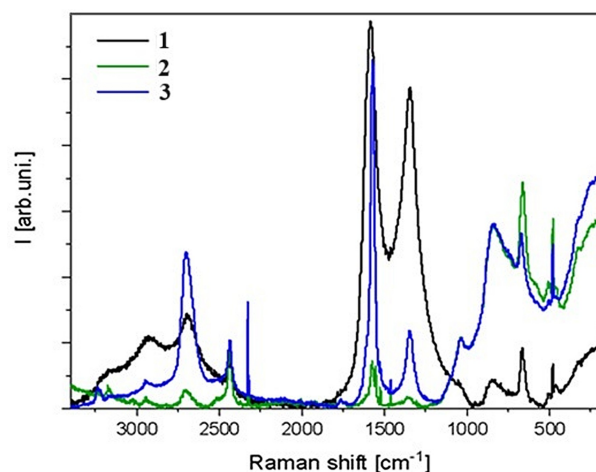


Figure 4. Raman spectra of the residue battery waste: Materials 1–3.

and graphite-specific (G bands) peaks are seen at Raman spectra, in particular at  $\sim 482\text{ cm}^{-1}$ ,  $\sim 1085\text{ cm}^{-1}$  (hardly discernible in Material 1),  $\sim 1347\text{ cm}^{-1}$  (D band),  $\sim 1576\text{ cm}^{-1}$  (G band),  $\sim 2331\text{ cm}^{-1}$ , the wide band  $\sim 2650\text{--}2900\text{ cm}^{-1}$  includes the 2D band ( $\sim 2680\text{ cm}^{-1}$ ). There are likely traces of heteroatoms and oxidized compounds responsible for some other bands.

Signals corresponding to  $-\text{CH}$  and  $\text{CH}_2$  deformation vibrations in the alkanes and alkenes, C–C stretching in alkene straight carbon chains, C–H in-plane deformation of substituted benzene, and in-phase  $-(\text{CH}_2)_n$  twisting may all be seen in the  $1000\text{--}1300\text{ cm}^{-1}$ . Additionally, peak  $\sim 3178\text{ cm}^{-1}$  is the most intense for Material 2,  $\sim 2323\text{ cm}^{-1}$  decreases significantly in Material 1 with respect to 2 and 3 where its intensity is comparable with this at  $2425\text{ cm}^{-1}$ , bands  $\sim 1460$ , and  $1525\text{ cm}^{-1}$  are in Material 2, and 3 (practically not observable in 1), and intensity of this  $\sim 184\text{ cm}^{-1}$  is higher for 2 than 1 and nearly absent in 3. That can be correlated with the lowest amount of heteroatoms and only traces of non-carbon compounds in Material 3. Assignments of the most prominent peaks are collected in Table S3.

The factors: the G/D ratio, the width at half-height, the presence and intensity of the 2D band, and RBS (Raman Band Separation), the difference between the positions of the G and D bands used for the evaluation of the quality of carbon materials,<sup>[60]</sup> presented in Table S4, confirmed that Material 3 is a highly ordered material with fewer defects. The average G to D (G/D) values together with different background cutoffs, were calculated from the total area of deconvoluted peaks and their intensity.

The G/D intensities ratio is considerably the highest in Material 3, with peaks narrow and well-separated, indicating the more structuralized morphology of carbon layers and the higher degree of graphitization. It also contains the  $\sim 3250\text{ cm}^{-1}$  weak bands typical for graphite reference materials. On the contrary, the broadening of the 2 D peak in Material 1 indicated the presence of numerous structural defects. Nearly the same 2D band position in all samples indicates no differences in

Table 1. Structural parameters of residue carbon-based Materials 1–3.		
Material	C ( <i>P63/mmc</i> ) <i>a</i> , <i>c</i> [Å]	%wt
Material 1	<i>a</i> = 2.4610(1) <i>c</i> = 6.7136(2)	90.1(7)
Material 2	<i>a</i> = 2.4611(1) <i>c</i> = 6.7128(2)	87.9(6)
Material 3	<i>a</i> = 2.4626(1) <i>c</i> = 6.7138(2)	92.0(7)

elongation or strain. In all Materials 2D:  $G < 1$  is typical for multilayered materials.

The difference between the positions of the D and G bands was used to calculate the RBS factor. RBS for Materials 1 and 3 is equal to  $232 \text{ cm}^{-1}$  and  $219 \text{ cm}^{-1}$ , respectively. Due to the bands overlapping, it may be roughly estimated to be in the range  $184\text{--}219 \text{ cm}^{-1}$  for Material 2. RBS differences may result from the layer stacking of the Materials, which has a lowering  $R_s$  for the G band, and rising compressive stress, which has a higher  $R_s$  for the D band.

To determine the pore size and volume of the studied Materials, Barret-Joyner-Halenda (BJH) analysis was performed. Material 3 exhibits the highest BET (Brunauer-Emmett-Teller) and BJH (surface area) values (Table 2) with a higher pore volume and a smaller pore size. This may result from the most developed fluffy structure (Figure 1e, f). Material 2 exhibits the lowest surface area, indicating a less developed structure, which is also seen in SEM images.

**ELECTROCHEMICAL STUDIES.** Next, the electrocatalytic ORR activity of the glassy carbon (GC) electrodes modified with different post-leached battery waste powders was examined by

	Material 1	Material 2	Material 3
BET ( $\text{m}^2 \text{g}^{-1}$ )	7.923	4.560	16.193
BJH <sub>ads</sub> Surface area, ( $\text{m}^2 \text{g}^{-1}$ )	6.402	5.056	13.904
BJH <sub>ads</sub> Pore volume ( $\text{cm}^3 \text{g}^{-1}$ )	0.018	0.0141	0.0217
BJH <sub>ads</sub> Pore size ( $\text{\AA}$ )	112.7	170.4	62.30

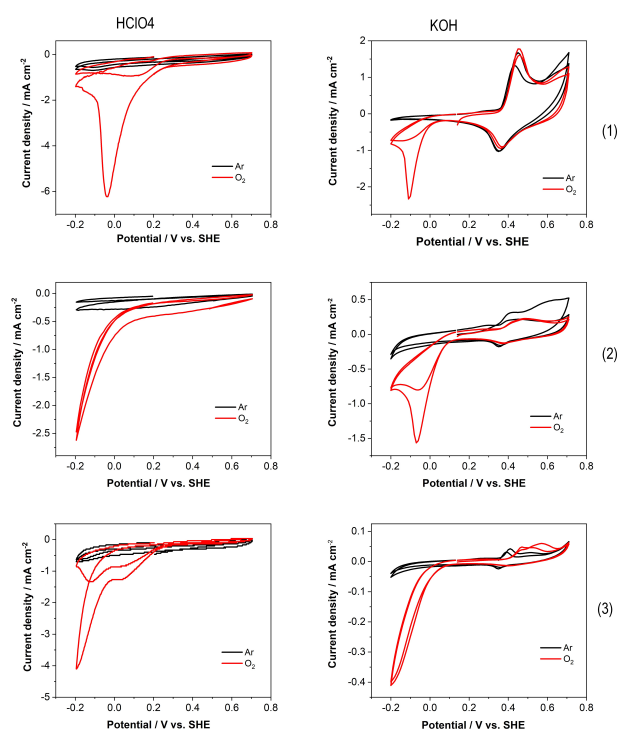


**Figure 5.** Cyclic voltammograms recorded for GC electrodes modified with Materials 1–3 in Ar- or  $\text{O}_2$ -saturated  $0.1 \text{ M HClO}_4$  (first column) or  $0.1 \text{ M KOH}$  (second column) aqueous solutions; scan rate:  $5 \text{ mV s}^{-1}$ .

CV performed in Ar- and  $\text{O}_2$ -saturated acidic and alkaline solutions (Figure 5). CV curves obtained in  $\text{O}_2$  and Ar atmospheres differ. For all tested Materials, the significant increase of cathodic current at c.a.  $0.2 \text{ V}$  (acidic solution) and c.a.  $0.05 \text{ V}$  (alkaline solution) is clearly seen in voltammograms recorded in  $\text{O}_2$ -saturated solutions (Figure 5, red curves). The ORR cathodic peaks of electrodes modified with Materials 1–3 were between  $-0.2 \text{ V}$  and  $-0.07 \text{ V}$  vs. SHE ( $0.5\text{--}0.64 \text{ V}$  vs. RHE) in alkaline media, which is more negative compared to pure rGO ( $0.73 \text{ V}$  vs. RHE)<sup>[61]</sup> and commercially used Pt/C ( $0.858 \text{ V}$  vs. RHE).<sup>[62]</sup> In an acidic solution, ORR peaks occurred between  $-0.2 \text{ V}$  and  $0 \text{ V}$  vs. SHE ( $0.5\text{--}0.7 \text{ V}$  vs. RHE), which is more negative in contrast to Pt-DPC ( $0.91 \text{ V}$  vs. RHE).<sup>[63]</sup> Moreover, there was a noticeable shift ( $0.1\text{--}0.2 \text{ V}$ ) in the onset potential in comparison to the bare GC electrode in the same conditions. (Figure S2). This effect is smaller in alkaline solutions and it is an indication of the ORR catalytic activity of LiBs' waste. The value of the onset potential and shape of the CV curve depend on the Material, which can be related to the morphology of the catalytic material, its wettability, and the distribution of the catalytic sites (see below). Two cathodic peaks seen on CV curves recorded with CG modified with Material 3 in an acidic solution may suggest a two-step ORR.<sup>[64]</sup> Cathodic currents corresponding to ORR are much higher for Materials 1 and 3 compared to Material 2, which may suggest that there are a larger number of defects in Material 1 or a higher graphitization level in Material 3.<sup>[65]</sup> The minor cathodic current increases at negative potentials (Figure 5, black curves) recorded in Ar-saturated solutions can be attributed to the hydrogen evolution.

In contrast to the acidic solution, a pair of the cathodic and anodic peaks appears on CV curves at  $0.3\text{--}0.6 \text{ V}$  recorded in both Ar- and  $\text{O}_2$ -saturated  $0.1 \text{ M KOH}$  solutions, which can be ascribed to  $\text{Co}^{2+}/\text{Co}^{3+}$  redox couple.<sup>[66,67]</sup> For electrodes modified with Material 3 another anodic peak is seen at ca.  $0.7\text{--}0.8 \text{ V}$ . Although the related cathodic peak is hardly visible, this signal may be ascribed to the  $\text{Co}^{3+}/\text{Co}^{4+}$  redox couple.<sup>[67]</sup> The presence of these voltammetric signals confirms the presence of redox-active cobalt oxide, as suggested above. The absence of this signal in an acidic solution results from the solubility in an acidic solution.<sup>[68]</sup>

To understand the ORR mechanism at LiBs' waste, LSV with RDE was performed (Figure S4). Based on the Koutecký-Levich (K–L) equation:

$$\frac{1}{i} = \frac{1}{i_k} + \frac{1}{B} \omega^{-1/2} \quad (1)$$

the number of transferred electrons ( $n$ ) per one oxygen molecule were calculated:<sup>[69]</sup>

$$n = \frac{B}{0.62FAD^{2/3} \nu^{-1/6} C_{\text{ox}}} \quad (2)$$

where  $i_k$ —kinetic current,  $\omega$ —electrode rotating rate (rpm),  $F$ —Faraday constant:  $96\,485 \text{ C mol}^{-1}$ ,  $A$ —electrode area:  $0.071 \text{ cm}^2$ ,  $D$ —diffusion coefficient:  $1.9 \times 10^{-5} \text{ cm}^2 \text{ s}^{-1}$  for  $\text{O}_2$  in  $0.1 \text{ M HClO}_4$  ( $1.98 \times 10^{-5} \text{ cm}^2 \text{ s}^{-1}$  in  $0.1 \text{ M KOH}$ ),<sup>[70]</sup>  $\nu$ —kinematic viscosity

( $0.01 \text{ m}^2 \text{ s}^{-1}$ ),<sup>[70]</sup> and  $C_{\text{ox}}$  is  $\text{O}_2$  concentration: ( $1.2 \times 10^{-3} \text{ mol dm}^{-3}$  in  $0.1 \text{ M HClO}_4$  and  $1.48 \times 10^{-3} \text{ mol dm}^{-3}$  in  $0.1 \text{ M KOH}$ ) at  $298 \text{ K}$ ).<sup>[70]</sup> For the rotation speed in  $\text{rad s}^{-1}$  unit, the constant  $B = 0.62$  was adopted.

For Material 3, ORR follows a 2-electron pathway both in an acidic and alkaline medium. The significant contribution of 4-electron oxygen reduction is seen for Materials 1 and 2 in alkaline and acidic electrolytes, respectively

(see Figure 6).

The relationship between LiBs' waste and its ORR electrocatalytic properties is not straightforward. It is known that the higher level of graphitization of carbon (here: Material 3 > Materials 2 > Material 1) increases its electronic conductivity, which enhances charge-transfer processes and facilitates 4-electron ORR.<sup>[71]</sup> Also, the higher level of topological defects (Material 1) has a similar effect.<sup>[72]</sup> However, some Authors demonstrated that carbon-based materials such as ordered mesoporous graphitic carbon, mildly reduced graphene oxide, and surface oxidized carbon nanotubes may exhibit 2-electron ORR in alkaline media.<sup>[73]</sup> Moreover, doping carbon-based materials with non-metal heteroatoms such as sulfur, fluorine, or nitrogen facilitates the 2-electron ORR path.<sup>[74–76]</sup> Although its role in the ORR mechanism is still being debated, it is believed that at doped carbon, the active sites on the carbon atoms adjacent to heteroatoms are generated and promote the breakage of  $\text{O}=\text{O}$  bonds following the oxygen binding energy modification.<sup>[77]</sup> Materials 1 and 3 contain a small amount of nitrogen, which may be the reason for their higher ORR catalytic activity compared to Material 2 (see below SECM). Furthermore, Materials 1 and 3 exhibit more porous, well-developed structures that may influence the mass transfer processes, enhancing their ORR catalytic ability.<sup>[78]</sup> Some theoretical and experimental research suggests that doping with the combination of the transition metal and non-metal of carbon materials may enhance their 4-electron ORR catalytic activity by accelerating the rupture of oxygen double bonds to  $\text{OOH}^*$  intermediate, which further forms  $\text{O}^*$  and  $\text{OH}^*$  resulting in the 4-electron ORR route. Therefore, enhancement of 2-electron ORR catalytic activity requires the design of active sites to minimize cleavage of the  $\text{OOH}^*$  bond which can be achieved by introduction oxygen-containing functionalities, such as carboxyl and epoxy groups, into the carbon-based materials.<sup>[73]</sup> In conclusion, application of acid leaching to recover spent LiBs' waste as well as the presence of nitrogen heteroatoms may increase the amount of oxygen functional groups<sup>[79]</sup> promoting 2-electron ORR at the residue carbon materials.

Finally, to eliminate the influence of the electrode and ionomer support<sup>[80]</sup> we focused on ORR at the same Materials assembled at the liquid-liquid interface.<sup>[34,80–83]</sup> For this purpose,  $2 \text{ mL}$  of a  $5 \text{ mM DMFc}$  solution in TFT was added to  $2 \text{ mL}$  of  $1 \text{ mg mL}^{-1}$  suspension of post-leached Li-ion powder in aqueous  $0.1 \text{ M HClO}_4$ .<sup>[34]</sup> The flask experiments demonstrated that all materials self-assembled at the liquid-liquid interface (Figure 7). In all cases: including the blank experiment (in the absence of LiBs' waste) the sample organic phase was yellow due to dissolved DMFc. However, after 3 h of experiments, the organic phase turned green in all vials containing battery waste

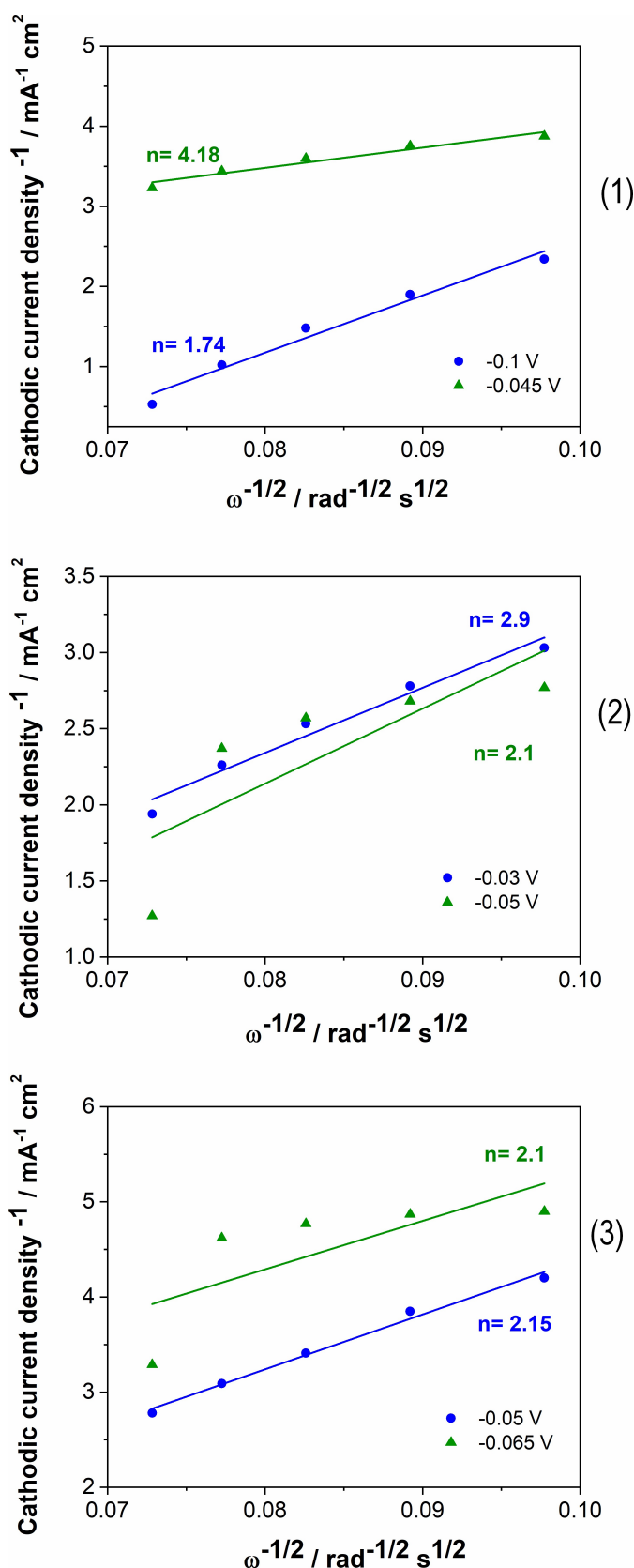
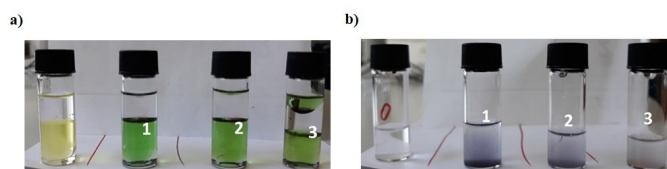


Figure 6. Koutecký-Levich plots for Materials 1–3 (Blue line  $0.1 \text{ M HClO}_4$ , green line  $0.1 \text{ M KOH}$ ) based on LSV recorded for GC electrode modified with Material 1–3 at various rotation rates (Figure S4).



**Figure 7.** a) Vials with 5 mM DMFc solution in TFT (bottom) and 0.1 M HClO<sub>4</sub> aq. (top) after 3 hours of experiment; and b) Aqueous phase collected from the vials after addition of KI and starch solutions. Numbers of vials corresponds to numbers of materials (0–blank).

(Figure 7a, 1–3), whereas no change of color was seen in a blank experiment (Figure 7a, vial on the left). The change in color (from yellowish to green) results from DMFc oxidation, which corresponds to DMFc<sup>+</sup> cations.<sup>[84]</sup> This indicates that biphasic ORR is accelerated by all studied LiBs' wastes.

To elucidate the mechanism of biphasic ORR, KI and starch solutions were added to the acidic aqueous phase collected from the glass vials after the experiment described above. Solutions collected from the experiment with LiBs' waste turned violet (Figure 7b, 1–3) due to the oxidation of iodide to triiodide by newly formed H<sub>2</sub>O<sub>2</sub> resulting in the formation of a purple complex of I<sub>3</sub><sup>-</sup> with starch.<sup>[84]</sup>

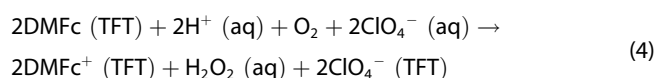
Next, SECM was employed to quantitatively estimate H<sub>2</sub>O<sub>2</sub> generation efficiency at the liquid-liquid interface. As in our previous study,<sup>[34]</sup> it was detected with the SECM approaching the liquid-liquid interface with 20 μm steps, activated by cyclic voltammetry in a wide potential range from −0.3 V to 1.3 V vs. the Ag wire quasi-reference electrode. The local concentration of H<sub>2</sub>O<sub>2</sub> (cH<sub>2</sub>O<sub>2</sub>) was estimated from the equation:

$$c\text{H}_2\text{O}_2 = \frac{i}{(4 \times n \times F \times D \times r)} \quad (3)$$

where  $n=2$ ,  $F$  - Faraday constant,  $D$  - diffusion coefficient  $D=8.8 \times 10^{-6} \text{ cm}^2 \text{ s}^{-1}$ ,<sup>[85]</sup> and  $r$  - radius of the microelectrode = 11.5 μm.

As the SECM tip approaches the liquid-liquid interface, cH<sub>2</sub>O<sub>2</sub> increases, indicating that 2-electron ORR occurs close to the liquid-liquid interface (Figure 8). It is significantly higher in the presence of battery waste at the interface. The estimated H<sub>2</sub>O<sub>2</sub> flux calculated from the slope of the approach curve is much higher for the battery waste modified interface: 0.11 nmol cm<sup>-2</sup> s<sup>-1</sup>,<sup>[34]</sup> 0.014 nmol cm<sup>-2</sup> s<sup>-1</sup> and 0.144 nmol cm<sup>-2</sup> s<sup>-1</sup> for Material 1, Material 2 and Material 3, respectively, as compared to the bare liquid-liquid interface (0.0055 nmol cm<sup>-2</sup> s<sup>-1</sup>).<sup>[34]</sup>

Due to the high (ca. 90%) degree of graphitization of LiBs' battery waste, the self-assembled film or at least some of its parts are electronically conductive. Therefore, one may say that during the biphasic ORR with DMFc as an electron donor:



electron is not necessarily directly transferred between O<sub>2</sub> and protonated DMFc molecules.<sup>[86]</sup> There is a significant contribu-

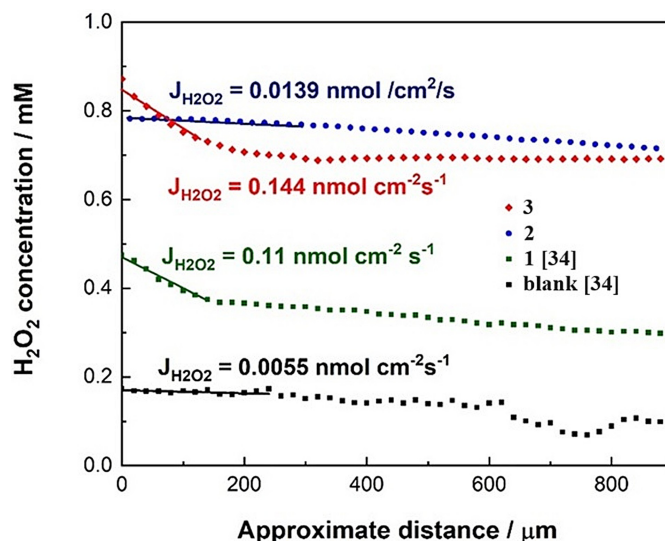


**Figure 8.** SECM approach curves recorded in the presence (red curve and blue curve) and absence (blue curve) of battery waste powder in a biphasic system as described above.

tion of electron transfer between these species approaching different sites of conductive particulate film. Perhaps O<sub>2</sub> molecules approach LiBs' waste film from both the "aqueous side" and the "organic side", whereas DMFc molecules approach only from the "organic side". The probability of such an event is obviously much higher than the encounter of three chemical species in the interfacial region. It must be emphasized that the effect of assembled carbon-based conductive materials (reduced graphene oxide, graphene) assembled at the liquid-liquid interface on ORR efficiency was earlier noted.<sup>[82,86]</sup> Importantly, the catalytic activity of Materials 1 and 3 towards biphasic ORR is one order higher than Material 2, which does not correlate with the degree of their graphitization, affecting LiBs' film conductivity. However, the value of this parameter (88–92%) does not depend much on the type of Material (Table 2) and the film conductivity may be similar. It also depends on the number of conductive paths formed, which certainly depends on the morphology of the Materials. Interestingly, the morphology of Material 2 is different than that of Materials 1 and 3. It may affect its wettability by aqueous and organic phases, thereby controlling the access of substrates to the conductive elements of the film. The other possibility for the differences in catalytic activity is the presence of cobalt oxides (see above). However, it does not correlate with the LiCoO<sub>2</sub> fraction in LiBs' waste (8–12% (Table 2)). Actually, materials with the highest content of cobalt oxides are less active. Overall, one may conclude that due to the number of factors affecting LiBs' waste catalytic activity towards biphasic ORR, the selection of the most important ones is hard at the moment.

In addition, the electrical conductivity of dried tablet-like Materials 1–3 was measured, and the results show similar values for all dried tablet-like samples (Table 3). The highest value for Material 2 may refer to a larger pore size, while the effect may differ in an aqueous solution also depending on the pH. At the

Material	d (cm)	I (mA)	Electrical conductivity (S cm <sup>-1</sup> )	Ref.
Carbon rode:elec-trode paste (9:0)	0.15	0.50	0.6889	[94]
		0.55	0.6804	
		0.60	0.6824	
Carbon rode:elec-trode paste (7:2)	0.14	0.50	2.7501	[94]
		0.55	2.7533	
		0.60	2.7535	
Porous hollow carbon spheres	0.125	0.0058	2.22	[95]
Material 1	0.22	0.50	2.44 ± 0.04	This work
		0.75	2.93 ± 0.02	
		1.00	3.35 ± 0.02	
Material 2	0.22	0.50	2.35 ± 0.03	This work
		0.75	2.91 ± 0.09	
		1.00	7.56 ± 1.12	
Material 3	0.24	0.50	2.47 ± 0.04	This work
		0.75	2.90 ± 0.05	
		1.00	3.51 ± 0.03	

same time, the graphitization is higher for Material 3, but lower pore sizes and cobalt-based compounds can cause lower electrical conductivity compared to Material 2. However, the results obtained with the four-probe setup are higher than the values presented in the literature for carbon-based materials, which is related to differences in the composition and structure of the leached materials (Table 3).

## Conclusions

The electrochemical results (CV, RDE, SECM) combined with surface composition analysis (SEM, XPS, Raman Spectroscopy, XRD, BET) uncovered the relationship between the morphology (nanostructures) and chemical composition of battery waste and its ORR catalytic capabilities. The obtained results also point out the role of unleached LiCoO<sub>2</sub> from LiBs' waste as a catalyst for electrochemical ORR. This approach may be useful for its recycling unless efficient and environmentally friendly recovery procedures are proposed.<sup>[87]</sup> This work confirmed the ORR catalytic properties of cobalt and graphitic-based materials. Moreover, it was shown that well-developed carbon nanostructures prompt oxygen reduction reaction. In addition, the research proved that the more structured morphology of carbon layers leads to a higher degree of graphitization (crystallinity), which also leads to increased oxygen reduction.

## Materials and Methods

**Materials.** HClO<sub>4</sub> (ACS reagent, 70%), α,α,α-trifluorotoluene (TFT) (anhydrous, ≥99%), Nafion 117 solution (~5% in a mixture of lower aliphatic alcohols and water) and glutaric acid (for synthesis, Merck KGaA) were purchased from Sigma Aldrich and were used as received. Decamethylferrocene (DMFc) (99%) was supplied by ABCR GmbH & Co KG (Germany) and KOH

(analytical grade) by POCH, H<sub>2</sub>O<sub>2</sub> (30% analytical grade) and H<sub>2</sub>SO<sub>4</sub> (96% analytical grade) were received from STANLAB (Lublin, Poland). Argon and oxygen gases (99.999% purity) were supplied by LINDE GAS POLAND. Deionized water purified with HYDROLAB with ion columns or with Arium® Comfort Lab Water System (Sartorius) was used to prepare solutions for CV and LSV experiments and SECM studies, respectively.

**Recovery of metals and carbon materials from spent Li-ion batteries by acid-leaching.** The substrate battery waste material was a mixed waste stream of spent laptop LiBs from various producers, including Samsung, HP, Acer, and Asus. Spent LiBs were mechanically disassembled and segregated into individual fractions. The anodic and cathodic masses of spent LiBs from various producers were mixed to obtain homogenous material, and to determine its composition, the ICP OES analysis was performed (Figure S6). Then, 10 g of dry anode and cathode powder was treated with 100 mL of leaching bath based on 5.0 M H<sub>2</sub>SO<sub>4</sub> aq. and containing reducing agents: H<sub>2</sub>O<sub>2</sub> or glutaric acid or both (see Table 4) for 2 h under stirring (c.a. 500 rpm) at 90 °C. The carbon residue was filtered and washed with deionized water (see<sup>[88]</sup> for details).

**The morphology and composition experiments.** The morphology of the recycled materials was characterized by the Scanning Electron Microscope (SEM) - FE-SEM Merlin (Zeiss) equipped with a Gemini II column (Stuttgart, Germany). This device worked in a low kV value range (0.5–1.5 kV) with a low probe current of 10–20 μA. Energy Dispersive X-ray Spectroscopy (EDS) was used for the elemental analysis of the solid Materials. The chemical composition of post-leaching residues was determined with X-ray Photoelectron Spectroscopy (XPS) using the Al Kα non-monochromated radiation (1486.6 eV) as a source with a maximum resolution of 0.83 eV (Microlab 350, Thermo Electron). X-ray Diffraction patterns were collected with a laboratory diffractometer (X'Pert Pro Alpha1 MPD, Panalytical) equipped with a Cu X-ray tube, a primary beam Ge (111) Johanson monochromator, and a position-sensitive linear semiconductor detector (X'Celerator). The Raman spectra were collected on DXR Raman Microscopy (Thermo Scientific) with the standard green laser line (532 nm, 10 mW). The exposure time was 12 s for Material 1 or 50 s for Materials 2 and 3, respectively. The aperture was 50 μm, and the repetition was 50 for each place (>10) tested materials. The average signal was then filtered, normalized, and the background cut off. For the spectra analysis, the following software: OMNIC (together with the libraries), ORIGIN and authors' Python scripts (signal deconvolution, peak search, and calculation of a surface area) were used. In addition, different background approaches:

Material 1	Material 2	Material 3
5.0 M H <sub>2</sub> SO <sub>4</sub> + 0.9% v/v H <sub>2</sub> O <sub>2</sub>	5.0 M H <sub>2</sub> SO <sub>4</sub> + 0.38 M glutaric acid C <sub>5</sub> H <sub>8</sub> O <sub>4</sub>	5.0 M H <sub>2</sub> SO <sub>4</sub> + 0.9% v/v H <sub>2</sub> O <sub>2</sub> + 0.38 M glutaric acid C <sub>5</sub> H <sub>8</sub> O <sub>4</sub>

OMNIC standard, adaptive iteratively reweighted penalized least squares (AIRPLS),<sup>[89]</sup> asymmetrically reweighted penalized least squares (ARPLS),<sup>[90]</sup> asymmetric least squares smoothing (ALSS) and its update,<sup>[91,92]</sup> were tested and compared, and the average quantitative parameters were taken. Brunauer-Emmett-Teller (BET) surface area analysis was conducted by ASAP 2020 - Micromeritics Instrument Corporation. Nitrogen adsorption/desorption were performed at 77 K. The electrical conductivity of the materials was measured using four-probe method using JANDEL RM3 setup.

**Electrochemical experiments** (cyclic voltammetry (CV) and linear sweep voltammetry (LSV)) were performed with Ivium potentiostat (Ivium Technologies, Netherlands) in a standard three-electrode cell. The static glassy carbon (GC) disc electrode (0.0314 cm<sup>2</sup>, Mineral, Poland) and GC rotating disc electrode (RDE) (0.071 cm<sup>2</sup>, Radiometer Analytical) served as working electrodes in CV and LSV experiments, respectively. The Ag|AgCl|KCl 3 M electrode (Mineral, Poland) or Hg/HgO electrode (Mineral, Poland)<sup>[90]</sup> were used as a reference electrode in acidic or alkaline media, respectively. Their potential was recalculated vs. the SHE electrode. As a counter electrode, platinum wire was employed in all experiments. GC electrodes were modified with the suspension of 10 mg battery waste powder suspended in 20 μL of 5% Nafion solution as recommended.<sup>[44]</sup> Voltammetric experiments were performed in 0.1 M HClO<sub>4</sub> and 0.1 M KOH aqueous solutions, after 30 min of purging either with Ar or O<sub>2</sub>. SECM with a Pt disc probe (11.5 μm radius, Goodfellow, England) was employed for the determination of H<sub>2</sub>O<sub>2</sub> at the liquid-liquid interface formed by DMFc solution in TFT and 0.1 M HClO<sub>4</sub> aqueous solution following the procedure applied in our preliminary study.<sup>[34]</sup> Pt microelectrodes were prepared by sealing a Pt wire in borosilicate capillaries using a Narishige PC-10 capillary puller.<sup>[93]</sup> The Rg ratio of the Pt tip was ca. 6.5. Before SECM experiments, Pt tips were polished with sandpaper and alumina slurry (0.3 μm and 0.05 μm).

## Supporting Information

Supporting Information contains some additional data concerning structural and composition analysis (XPS, XRD, Raman Spectroscopy, BET) and electrochemical studies (CVs for bare GC electrodes and LSV measurements for GC modified with battery waste Materials).

## Acknowledgements

M. Warczak would like to thank the National Science Center (NCN, Poland) for financial support through grant SONATA No. 2022/47/D/ST4/01421. A. Dabrowska's contribution was supported by the University of Warsaw miniDUB "Ilościowa i jakościowa analiza widm Ramana zanieczyszczeń środowiskowych i materiałów węglowych z recyklingu"; BOB-661-1427/2023. M. Osial would like to thank Dr. Bożena Sikora from the Institute of Physics, Polish Academy of Science for consultations, Kamil Bochenek from Institute of Fundamental Technological

Research, Polish Academy of Sciences for technical support, and Marcin Strawski from Department of Chemistry, University of Warsaw for an access to the equipment. M. Opallo would like to acknowledge the National Science Centre (NCN, Poland) for financial support through grant UNISONO Solar-Driven Chemistry No. 2019/01/Y/ST4/00022. M. Warczak would like to thank Katarzyna Belka (Bydgoszcz University of Science, Faculty of Chemical Technology and Engineering) for her help and technical support in the laboratory. A. Dabrowska is grateful to Piotr Machowski (help in the programming and design of Python scripts).

## Conflict of Interests

The authors declare no conflict of interest.

## Data Availability Statement

The data that support the findings of this study are available from the corresponding author upon reasonable request.

**Keywords:** Lithium-ion battery · recycling · electrocatalysis · oxygen reduction · hydrogen peroxide

- [1] C. Hu, L. Dai, *Adv. Mater.* **2017**, *29*, 1604942.
- [2] S. T. Rahman, K. Y. Kyong, S. J. Park, *Nanotechnol. Rev.* **2022**, *10*, 137–157.
- [3] A. Damjanovic, M. A. Genshaw, J. O. M. Bockris, *J. Electrochem. Soc.* **1967**, *114*, 1107–1112.
- [4] H. S. Wroblowa, Y. C. Pan, G. Razumney, *J. Electroanal. Chem.* **1976**, *69*, 195–201.
- [5] Y. Wu, R. Holze (Eds), *Electrochemical Energy Conversion and Storage*. Wiley, Weinheim **2022**, 261.
- [6] E. Miglbauer, P. J. Wojcik, E. D. Glowacki, *Chem. Commun.* **2018**, *54*, 11873.
- [7] J. M. Campos-Martin, G. Blanco-Brieva, J. L. G. Fierro, *Angew. Chem. Int. Ed.* **2006**, *45*, 6962–6984.
- [8] N. Wang, Sh. Ma, P. Zuo, J. Duan, B. Hou, *Adv. Sci.* **2021**, *8*, 2100076.
- [9] Y. Wang, G. I. N. Waterhouse, G. L. Shang, T. Zhang, *Adv. Energy Mater.* **2021**, *11*, 2003323.
- [10] Y. Zhang, M. Luo, Y. Yang, Y. Li, S. Guo, *ACS Energy Lett.* **2019**, *4*, 1672–1680.
- [11] S. Sui, X. Wang, X. Zhou, Y. Yuehong Su, S. Riffat, Ch.-j. Liu, *J. Mater. Chem. A* **2017**, *5*, 1808–1825.
- [12] Y. Wang, J. Li, Z. Wei, *J. Mater. Chem. A* **2018**, *6*, 8194–8209.
- [13] Y. Li, Q. Li, H. Wang, L. Zhang, D. P. Wilkinson, J. Zhang, *Electrochem. Energy Rev.* **2019**, *2*, 518–538.
- [14] X. Zhao, H. Su, W. Cheng, H. Zhang, W. Che, F. Tang, Q. Li, *ACS Appl. Mater. Interfaces* **2019**, *11*, 34854–34861.
- [15] Y. Wang, W. Zhou, J. Gao, Y. Ding, K. Kou, *J. Electroanal. Chem.* **2019**, *833*, 258–268.
- [16] J. Quilez-Bermejo, E. Morallón, D. Cazorla-Amorós, *Carbon* **2020**, *165*, 434–454.
- [17] A. Byeon, W. Ch. Yun, J. M. Kim, J. W. Lee, *Chem. Eng. J.* **2023**, *456*, 141042.
- [18] K. Ri, S. Pak, D. Sun, Q. Zhong, S. Yang, S. Sin, L. Wu, Y. Sun, H. Cao, H. Ch. Han, Ch. Xu, Y. Liu, H. He, S. Li, Ch. Sun, *Appl. Catal. B* **2024**, *343*, 123471.
- [19] H. Hu, G.-H. Gao, B.-B. Xiao, P. Zhang, J.-L. Mi, *Diamond Relat. Mater.* **2023**, *134*, 109776.
- [20] D. Wieczorek, D. Kwaśniewska, *Phys. Sci. Rev.* **2018**, *3*, 20180027.
- [21] Z. J. Baum, R. E. Bird, X. Yu, J. Ma, *ACS Energy Lett.* **2022**, *7*, 712–719.
- [22] P. Xu, D. H. S. Tan, B. Jiao, H. Gao, X. Yu, Z. Chen, *Adv. Funct. Mater.* **2023**, *33*, 2213168.

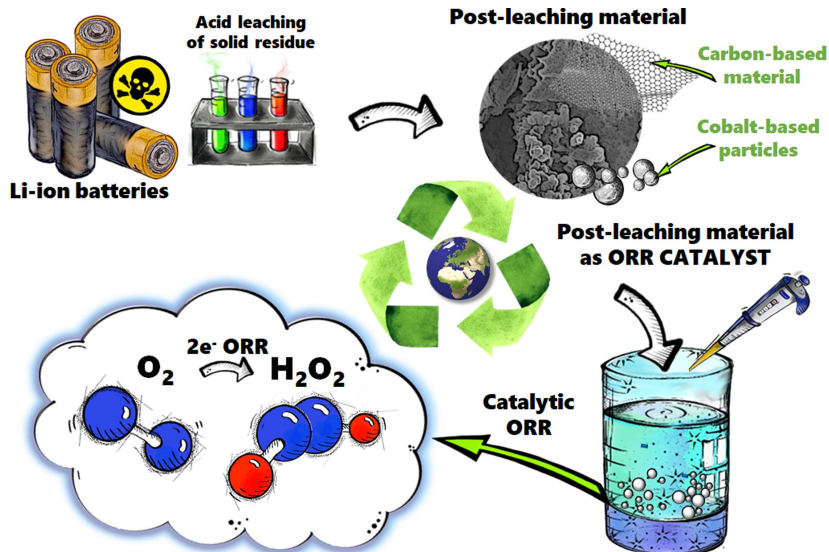
- [23] M. S. Shin, N. H. Kim, J. S. Sohn, D. H. Yang, Y. H. Kim, *Hydrometallurgy* **2005**, *79*, 172–181.
- [24] L. F. Zhou, D. Yang, T. Du, H. Gong, W. B. Luo, *Front. Chem.* **2020**, *8*, 1027.
- [25] D. Steward, A. Mayyas, M. Mann, *Procedia Manuf.* **2019**, *33*, 272–279.
- [26] N. Vieceli, R. Casasola, G. Lombardo, B. Ebin, M. Petranikova, *Waste Manage.* **2021**, *125*, 192–203.
- [27] X. Chen, H. Ma, C. Luo, T. Zhou, *J. Hazard. Mater.* **2017**, *326*, 77–86.
- [28] F. Meng, Q. Liu, R. Kim, J. Wang, G. Liu, A. Ghahreman, *Hydrometallurgy* **2020**, *191*, 105160.
- [29] G. P. Nayaka, Y. Zhang, P. Dong, D. Wang, Z. Zhou, J. Duan, X. Li, Y. Lin, Q. Meng, K. V. Pai, J. Manjanna, G. Santhosh, *J. Environ. Chem. Eng.* **2019**, *7*, 102854.
- [30] P. Meshram, Abhilash, B. D. Pandey, T. R. Mankhand, H. Deveci, *J. Met.* **2016**, *68*, 2613–2623.
- [31] W. Urbańska, *Minerals* **2020**, *10*, 555.
- [32] C. Peng, J. Hamuyuni, B. P. Wilson, M. Lundström, *Waste Manage.* **2018**, *76*, 582–590.
- [33] K. S. Bejigo, S. Natarajan, K. Bhunia, V. Elumalai, S.-J. Kim, *J. Cleaner Prod.* **2023**, *384*, 135520.
- [34] M. Warczak, M. Osial, W. Urbanska, M. Pisarek, W. Nogala, M. Opallo, *Electrochem. Commun.* **2022**, *136*, 107239.
- [35] A. Dessalle, J. Quílez-Bermejo, V. Fierro, F. Xu, A. Celzard, *Carbon* **2023**, *203*, 237–260.
- [36] M. Borghei, J. Lehtonen, L. Liu, O. J. Rojas, *Adv. Mater.* **2018**, *30*, 1703691.
- [37] Ch. Sathiskumar, L. Meesala, P. Kumar, B. Ramachandra Rao, N. S. John, H. S. S. Ramakrishna Matte, *Sustain. Energy Fuels* **2021**, *5*, 1406–1414.
- [38] S. A. Mirshokraee, M. Muhyuddin, R. Morina, L. Poggini, E. Berretti, M. Bellini, A. Lavacchi, C. Ferrara, C. Santoro, *J. Power Sources* **2023**, *557*, 232571.
- [39] M. Kazemi, K. Liivand, M. Prato, P. Vacek, J. Walmsley, S. Dante, G. Divitini, I. Kruusenberg, *Energy Fuels* **2024**, *38*, 659–670.
- [40] K. Liivand, M. Kazemi, P. Walke, V. Mikli, M. Uibu, *ChemSusChem* **2021**, *14*, 1103–1111.
- [41] K. Liivand, J. Sainio, B. P. Wilson, I. Kruusenberg, M. Lundström, *Appl. Catal. B* **2023**, *332*, 122767.
- [42] Y. Shen, G. Zhang, R. Wang, L. Shen, Q. Li, F. Zheng, Q. Wu, Z. Ma, *ChemPlusChem* **2022**, *87*, e202200328.
- [43] M. Opallo, K. Dusilo, M. Warczak, J. Kalisz, *ChemElectroChem* **2022**, *9*, e202200513.
- [44] Ch. Wei, R. R. Rao, J. Peng, B. Huang, I. E. L. Stephens, M. Risch, Z. Xu, Y. Shao-Horn, *Adv. Mater.* **2019**, *31*, 1806296.
- [45] B. Su, R. Partovi Nia, F. Li, M. Hojeij, M. Prudent, C. Corminboeuf, Z. Samec, H. H. Girault, *Int. Angew. Chem. Edit.* **2008**, *47*, 4675–4678.
- [46] A. Dąbrowska, W. Urbańska, M. Warczak, M. Osial, *Phys. Status Solidi B* **2022**, *259*, 2100588.
- [47] M. Michalska, P. Ławniczak, T. Strachowski, A. Ostrowski, W. Bednarski, *Beilstein J. Nanotechnol.* **2022**, *13*, 1473–1482.
- [48] J. Asenbauer, T. Eisenmann, M. Juenzel, A. Kazzazi, Z. Chen, S. Bresser, *Sustain. Energy Fuels* **2020**, *4*, 5387.
- [49] B. Lesiak, L. Kövér, J. Tóth, J. Zemek, P. Jiricek, A. Kromka, N. Rangam, *Appl. Surf. Sci.* **2018**, *452*, 223–231.
- [50] D. V. Sivkov, O. V. Petrova, S. V. Nekipelov, A. S. Vinogradov, R. N. Skandakov, S. I. Isaenko, A. M. Ob'edkov, B. S. Kaverin, I. V. Vilkov, R. I. Korolev, V. N. Sivkov, *Nanomaterials* **2021**, *11*, 2993.
- [51] R. Zhu, Q. Tao, M. Lian, X. Feng, J. Liu, M. Xe, X. Wang, S. Dong, T. Cui, P. Zhu, *Materials* **2019**, *12*, 1780.
- [52] Y. Liu, H. Jiang, C. Liu, Y. Ge, L. Wang, B. Zhang, H. He, S. Liu, *Atmos. Chem. Phys.* **2019**, *19*, 8175–8187.
- [53] T. S. Pathan, M. Rashid, M. Walker, W. D. Widanage, E. Kendrick, *J. Phys. E* **2019**, *1*, 044003.
- [54] G. E. P. O'Connell, T. H. Tan, J. A. Yuwona, Y. Wang, A. Kheradmand, Y. Jiang, P. V. Kumar, R. Amal, J. Scott, E. C. Lovell, *Appl. Catal. B* **2024**, *343*, 123507.
- [55] M. C. Biesinger, B. P. Payne, A. P. Grosvenor, L. W. M. Lau, A. R. Gerson, R. St. C. Smart, *Appl. Surf. Sci.* **2011**, *257*, 2717–2730.
- [56] M. Fantauzzi, B. Elsener, D. Atzei, A. Rigoldi, A. Rossi, *RSC Adv.* **2015**, *95*, 75953–75963.
- [57] A. S. Singh, J. H. Advani, A. V. Biradar, *Dalton Trans.* **2020**, *21*, 7210–7217.
- [58] H. Wang, W.-D. Zhang, Z.-Q. Deng, M.-C. Chen, *Solid State Ionics* **2009**, *180*, 212–215.
- [59] J. T. Hertz, Q. Huang, T. McQueen, T. Klimczuk, J. W. G. Bos, L. Viciu, R. J. Cava, *Phys. Rev. B* **2008**, *77*, 075119.
- [60] L. M. Malard, M. A. Pimenta, G. Dresselhaus, M. S. Dresselhaus, *Phys. Rep.* **2009**, *473*, 51–87.
- [61] H. Gai, S. Xue, X. Wang, J. Zhou, H. Jiang, M. Huang, *Mater. Today Energy* **2021**, *21*, 100809.
- [62] Y. Wu, L. Ge, A. Veksha, G. Lisak, *Nanoscale* **2020**, *12*, 13028–13033.
- [63] Y. Dong, Y. Wang, Z. Tian, K. Jiag, Y. Li, Y. Lin, C. W. Oloman, E. L. Gyenge, J. Su, L. Chen *The Innovation* **2021**, *2*, 100161.
- [64] A. Roguska, A. Leśniewski, M. Opallo, W. Nogala, *Electrochem. Commun.* **2021**, *133*, 107167.
- [65] S. Zhu, Y. Huang, T. Yu, Y. Lei, X. Zhu, T. Yang, J. Gu, C. Wang, *Int. J. Hydrogen Energy* **2024**, *51* (Part C), 956–965.
- [66] K. Ismail, W. Badawy, *J. Appl. Electrochem.* **2000**, *30*, 1303–1311.
- [67] B. Han, D. Qian, M. Risch, H. Chen, M. Chi, Y. S. Meng, Y. Shao-Horn, *J. Phys. Chem. Lett.* **2015**, *6*, 1357–1362.
- [68] M. Pourbaix, *Atlas d'Equilibres Electrochimiques*, GauthiersVillars, Paris **1963**.
- [69] A. J. Bard, L. R. Faulkner, *Electrochemical Methods: Fundamentals and Applications*, 2<sup>nd</sup> ed., J. Wiley, and Sons, **2001**, New York, p.341.
- [70] M. Yang, H. Chen, D. Yang, Y. Gao, H. Li, *RSC Adv.* **2016**, *6*, 97259–97265.
- [71] L. Li, P. Dai, X. Gu, Y. Wang, L. Yan, X. Zhao, *X J. Mater. Chem. A* **2017**, *5*, 789–795.
- [72] H. N. Fernandez-Escamilla, J. Guerrero-Sanchez, E. Contreras, J. M. Ruiz-Marizcal, G. Alonso-Nunez, O. E. Contreras, R. M. Felix-Navarro, J. M. Romo-Herrera, N. Takeuchi, *Adv. Energy Mater.* **2021**, *11*, 2002459.
- [73] W. Liu, J. Feng, R. Yin, Y. Ni, D. Zheng, W. Que, X. Niu, X. Dai, W. Shi, F. Wu, J. Yang, X. Cao, *Chem. Eng. J.* **2022**, *430* (3), 132990.
- [74] M. Vikkisk, I. Kruusenberg, U. Joost, E. Shulga, I. Kink, K. Tammeveski, *Appl. Catal. B* **2014**, *147*, 369–376.
- [75] W. Wang, X. Lu, P. Su, Y. Li, J. Cai, Q. Zhang, M. Zhou, O. Arotiba, *Chemosphere* **2020**, *259*, 127423.
- [76] G. Ye, M. Tian, S. Liu, Z. He, *ChemCatChem* **2024**, *16*, e202301345.
- [77] X. Ge, A. Sumboja, D. Wu, T. An, B. Li, F. W. T. Goh, T. S. A. Hor, Y. Zong, Zh. Liu, *ACS Catal.* **2015**, *5*, 4643–4667.
- [78] H. Yu, L. Shang, T. Bian, R. Shi, G. I. N. Waterhouse, Y. Zhao, Ch. Zhou, L.-Z. Wu, Ch.-H. Tung, T. Zhang, *Adv. Mater.* **2016**, *25*, 5080–6.
- [79] M. Jerigová, M. Odziomek, N. López-Salas, *ACS Omega* **2022**, *7*, 11544–11554.
- [80] P. Peljo, M. D. Scanlon, A. J. Olaya, L. Rivier, E. Smirnov, H. H. Girault, *J. Phys. Chem. Lett.* **2017**, *8* (15), 3564–3575.
- [81] E. Smirnov, P. Peljo, M. D. Scanlon, H. H. Girault, *Electrochim. Acta* **2016**, *197*, 362–373.
- [82] A. N. J. Rodgers, R. A. W. Dryfe, *ChemElectroChem.* **2016**, *3*, 472–479.
- [83] T. J. Stockmann, L. Angele, V. Brasiliense, C. Combellas, F. Kanoufi, *Angew. Chem. Int. Ed.* **2017**, *56*, 13493–13497.
- [84] W. Adamiak, J. Jedraszko, W. Nogala, M. Jönsson-Niedziolka, S. Dongmo, G. Wittstock, H. H. Girault, M. Opallo, *J. Phys. Chem. C.* **2015**, *119*, 20011–20015.
- [85] M. A. Komkova, A. Pasquarelli, E. A. Angreew, A. A. Galushin, A. A. Karyakin, *Electrochim. Acta* **2020**, *339*, 135924.
- [86] S. Rastgar, H. Deng, F. Cortez-Salazar, M. D. Scanlon, M. Pribil, V. Amstutz, A. A. Karyakin, S. Sharokhian, H. H. Girault, *ChemElectroChem* **2014**, *1*, 59–63.
- [87] Y. Chen, Y. Lu, Z. Liu, L. Zhou, Z. Li, J. Jang, L. Wei, P. Ren, T. Mu, *ACS Sustainable Chem. Eng.* **2020**, *8*, 11713–11720.
- [88] W. Urbańska, M. Osial, *Energies* **2020**, *13*, 6732.
- [89] Z.-M. Zhang, S. Chen, Y.-Z. Liang, *Analyst* **2010**, *135*, 1138–1146.
- [90] S.-J. Baek, A. Park, Y.-J. Ahna, J. Choo, *Analyst* **2015**, *140*, 250.
- [91] H. F. M. Boelens, P. H. C. Eilers, T. Hankemeier, *Anal. Chem.* **2005**, *77*, 7998–8007.
- [92] S. He, Z. Wie, L. Lijuan, H. Yu, H. Jiming, X. Wanyi, W. Peng, D. Chunlei, *Anal. Methods* **2014**, *6*, 4402–44.
- [93] J. Jedraszko, W. Nogala, W. Adamiak, S. Dongmo, G. Wittstock, H. H. Girault, M. Opallo, *Chem. Commun.* **2015**, *51*, 6851–6853.
- [94] S. Handaja, H. Susanto, Hermawan, *Int. J. Renew. Energy Develop.* **2021**, *10* (2), 221–227.
- [95] K. Zhang, Q. Zhao, T. Zhanliang, J. Chen, *Res. Nano* **2013**, *6* (1), 38–46.

Manuscript received: March 19, 2024

Revised manuscript received: April 27, 2024

Version of record online: ■■, ■■

# RESEARCH ARTICLE



This paper demonstrates the utilization of Li-ion battery waste as an efficient electrocatalyst for ORR. The studies show that the waste powder compositions and structures, e.g.,

porosity, heteroatom presence, level of defects, and graphitization, have a significant impact on its catalytic activity towards 2-electron ORR.

*Ph. D. M. Warczak\*, Ph. D. M. Osial, Ph. D. W. Urbańska, B. Eng. N. Sławkowska, Ph. D. A. Dąbrowska, Ph. D. M. Bonarowska, Ph. D. Eng. M. Pisarek, Ph. D. R. Minikayev, Prof. M. Giersig, Prof. M. Opallo*

1 – 11

**Insights Into the High Catalytic Activity of Li-ion Battery Waste Toward Oxygen Reduction to Hydrogen Peroxide**

